Structural, morphological, optical and magnetic properties of $Cu_{1-x}Ni_xFe_2O_4$ nanoferrites

Talaat M. Hammad [1*], **Nasser K. Hejazy** [2]

[1] Physics Department, Faculty of Science, Al-Azhar University, P.O. Box 1277, Gaza, Palestine
[2] Technology & applied Sciences, Al-Quds Open University, Gaza Branch, Gaza, Gaza Strip, Palestine

IJASR 2021
VOLUME 4
ISSUE 6 NOVEMBER – DECEMBER **ISSN: 2581-7876**

Abstract: $Cu_{1-x}Ni_xFe_2O_4$ ($0 \leq x \leq 1$) nanoferrites were organized by means of co-precipitation technique. The influence of Ni^{2+} substitutions on the structure, morphological, optical, magnetic properties of $Cu_{1-x}Ni_xFe_2O_4$ nanoferrites were studied. XRD patterns of synthesized samples exhibit the single-phase formation of spinel crystalline structure besides any trace of impurity. The substitution of Ni^{2+} in $Cu_{1-x}Ni_xFe_2O_4$ outcomes in a minimize of particle size from 20 to 11 nm. In addition, the lattice constant always decreased from 8.362 to 8.345 8 Å by increasing the concentration of Ni^{2} ions. Particle sizes obtained from TEM micrographs correspond to crystallite size calculated in the XRD results. The FTIR spectra of $Cu_{1-x}Ni_xFe_2O_4$ display two primary extensive metal-oxygen bands. The band gap energy of nanoferrites will increase from 3.32 to 3.62 eV with an increase the content of Ni^{2+} ions. The magnetic properties of the samples were measured using a superconductive quantum interferometer (SQUID) system at room temperature. The findings showcase that the magnetic properties of copper ferrite are noticeably impacted by the amount of Ni^{2} ions doping. When the quantity of nickel ions increases, the saturation magnetization increases as seen from the M-H loops.

Keywords: Magnetic; Optical properties; Magnetic properties; Nickel Nano Ferrites.

1 Introduction

Magnetic nanoparticles have been extensively studied in recent years, and these ferrites form an integral class of materials due to their peculiar magnetic and electrical properties [1]. Because of their large surface to volume ratio, ferrite nanoparticles exhibit fascinating and significantly different magnetic properties than those of bulk materials. These magnetic particles have been commonly used in specific fields such as magnetic media, electronic devices, gas sensors, drug delivery, microwave absorbent, catalyst, hyperthermia, magnetic resonance imaging, ferrofluids, lithium-ion batteries, magnetic diagnostics, etc.[2-6]. MFe_2O_4 (where M(II) = Fe(II), Mn(II), Co(II), Ni(II)) spinel ferrite nanoparticles are often used for contrast improvements in magnetic storage systems, photomagnetic materials and magnetic resonance imaging (MRI), especially drug delivery and hyperthermia[7-10]. The composition of the ferrites is based on the chemical classification of the divalent metal (MII) and the size and distribution of the metal ions at the tetrahedral and octahedral sites of the spinal structure [11, 12]. For spinel ferrites, MFe_2O_4 is a general formula where M is a divalent metal ion and Fe is present in the state of +3 oxidation

[13-16]. There are usually two types of structures of spinel ferrite: the normal and the inverse [17,18]. The occupied tetrahedral sites include the M^{2+} ions in the usual spinel, while the Fe^{3+} ions are located in the octahedral sites occupied [19,20].

Nevertheless, in the occupied octahedral sites, all M^{2+} ions and half of the Fe^{3+} ions are found, with the other half of the Fe^{3+} ions in the inverse spinel occupied at the tetrahedral sites. The substitution of various magnetic ions at sites A and B has a powerful effect on the properties of the ferrites. The great variations in physical characteristics were due to the ability to deal with metal ions and their distribution at the available sites. The basic class of spinel structure ferrites [21] is nickel copper ferrite. The magnetic interaction and ion distribution of tetrahedral lattice sites and octahedral lattice sites influence the structural and magnetic properties of spinel ferrites [22]. Nickel copper ferrites are soft spinel ferrites which are used in multilayer chip inductor applications due to their high electrical resistivity, chemical stability and exceptional magnetic properties at high frequencies [23]. This composition is represented by the (Fe^{+3}) $(Ni^{+2}Fe^{+3})O_4$, half of the iron atoms occupy the tetrahedral sites (A) and half of the magnetic atoms occupy the octahedral sites (B). In this structure, the tetrahedral site (A site) is entirely occupied by Fe3+, even as the octahedral site (B site) is occupied by Fe^{3+} and Ni^{2+}ions. This illustrates ferrimagnetism at the octahedral level as a consequence of antiparallel spins on the tetrahedral site between Fe^{3+} and Ni^{2+}. This illustrates

ferrimagnetism at the octahedral level as a consequence of antiparallel spins on the tetrahedral site between Fe^{3+} and Ni^{2+}. It is well known that the physical properties of the spinel ferrites are very sensitive to the preparation process. A key to obtaining good quality ferrite nanoparticles [24] is the selection of an effective synthesis process. For the synthesis of nickel copper mixed ferrite nanoparticle, various processes such as chemical co-precipitation, sol-gel, ball milling, citrate precursor, mechanochemical, glycine nitrate, adjusted oxidation, hydrothermal, solid state, etc. are mentioned in the literature [25-28].

Among both of these processes, co-precipitation was favored. This includes the simultaneous precipitation of two or more metal salts in a solution, the use of a precipitating agent (or ligand) and the subsequent thermal decomposition of the precipitate [29]. Compared to other methods, it provides many advantages, such as better distribution of contributors in the generated ferrites, low cost and good control of stoichiometry [30,31]. Several studies [32-34] have recorded high replacement rates, with an increase in the Ni content of $CuFe_2O_4$ contributing to an increase in magnetization. For example, Saleem et al. [33], by co-precipitation technique, prepared $Cu_{1-x}Ni_xFe_2O_4$ nanoparticles to test the absorption properties of electromagnetic (EM) waves.

He confirmed the formation of a single-phase cubic structure and disclosed that the saturation magnetization increases with the addition of Ni material. Doha et al. [34] prepared $Cu_{1-x}Ni_xFe_2O_4$ nanopowders using the co-precipitation ultrasonic irradiation technique. $Cu_xNi_{1-x}Fe_2O_4$ single-phase nanopowders with grain sizes ranging from 20 to 30 nm have been obtained. At x= 0.5, the maximum magnetization saturation value obtained was 73.5 emu / g. By using the sol-gel auto-combustion process, Azadmanjiri et al. [35] synthesized $Cu_xNi_{1-x}Fe_2O_4$ nanoferrites.

The Cu material has been reported to have a major influence on electromagnetic properties. Roumaih [36] synthesized $Cu_xNi_{1-x}Fe_2O_4$ using the standard ceramic process. The section pureness of the samples was studied by XRD and IR spectroscopy. To study the magnetic properties of $Cu_xNi_{1-x}Fe_2O_4$, prepared using the standard ceramic process, Msomi and Moyo [37] used Mössbauer spectroscopy and VSM techniques. XRD has confirmed the compound's single-phase formation. The coercive area (Hc) was found to increase with the decrease in grain size.
XRD has reported single-phase formation of the compound. With the reduction in grain size the coercive area (H_c) has been found to increase. In our previous studies, we have documented [38] the role of zinc substituted on the physical properties of copper ferrites nanoparticles prepared by co-precipitation chemical method. Although a lot of work has been done on of $Cu_xNi_{1-x}Fe_2O_4$, however, a little work done on in the optical and magnetic properties of $Cu_{1-x}Ni_xFe_2O_4$ nanoferrites is reported in previous literature.

The present work identifies the preparation of Ni doped copper ferrite nanoparticles with composition $Cu_{1-x}Ni_xFe_2O_4$ (x= 0.2, 0.4, 0.6, 0.8 and 1.0) by using precipitation method. The effect of the replacement of nickel ions on the structural, magnetic, and optical properties of nanoparticles of copper ferrite has been studied.

2. Experimental

2.1 Materials and methods

Therefore, $Cu_{1-x}Ni_xFe_2O_4$ ($0 \leq x \leq 1$) nanoferrites have been prepared using the precipitation method [38], as previously described. Nickel sulfate hexahydrate, $NiSO_4.6H_2O$, copper sulfate pentahydrate, $CuSO_4.5H_2O$ and ferrous ammonium sulfate hexahydrate, , $(NH_4)_2Fe(SO_4)_2.6H_2O$ were sooner or later dissolved in 25 mL of deionized water as preferred stoichiometric element amounts. The reaction mixtures were vigorously and continuously agitated for 60 min using magnetic stirring. 20 mmol of oxalic acid dissolved in an equal volume of deionized water and delivered dropwise for 60 min to metallic salts below magnetic stirring. A precipitate of (Cu, Ni, Fe) oxalate is removed, washed with water several times, and dried at 100oC for 24 hours. The yield of the pattern was then poured into a mortar and pestle gate using fine powder. The powder was annealed at 500°C for 3 hours in the muffle furnace to form $Cu_{1-x}Ni_xFe_2O_4$.

2.2 Characterization

The X-ray diffractometer (XRD) powder was used to confirm the crystal structure reported at room temperature on the X-ray diffractometer XDS 2000, Scintac Inc., USA, fitted with CuK wavelength (λ=1.5Å) radiation. For chemical analysis, the Fourier-transform infrared spectroscopy (Frontier Perkin Elmer) spectrophotometer in the

400-200 cm^{-1} frequency range was used to validate the chemical bonds present in the sample. For the determination of optical absorption properties and band gap energy, UV-Vis absorption spectroscopy (Hewlett Packard 8453) was used. For luminescence tests, a fluorescence spectrophotometer (Perkin- Elmer LS 50B) was used. A Tecnai F300 transmission electron microscopy (TEM) was used to investigate the morphological studies of prepared nanoparticles. Via comprehensive field-dependent magnetization measurements in fields up to 40 KOe on (SQUID) Quantum Design MPMS XL-7 magnetometer in RSO mode, magnetisms of synthesized nanoferrites were investigated.

3 Results and Discussion

3.1 Structural analysis

XRD patterns of $Cu_{1-x}Ni_xFe_2O_4$ are displayed in Fig. 1. The XRD spectra of the samples display diffraction peaks (2θ) at angles of 29.8°, 35.46°, 43.74°, 53.86°, 56.78°, and 62.32° may be assigned to the reflections of (220), (311), (400), (422), (511) and (440) planes, respectively. All the XRD peaks located might be traced to cubic spinel lattice indicating their single-phase structure without the presence of other impurity phases (e.g. Fe_2O_3, NiO, CuO etc.). Enhancing the Ni content causes the intensity of peaks to decrease as seen more clearly for (311) signals. The narrow sharp peaks propose that the $Cu_{1-x}Ni_xFe_2O_4$ products are crystalline, suggesting that this method of synthesize is used to gain the excessive purity of synthesized nanoferrites

[39–41]. It is found that the peaks of diffraction widened with increased concentration of Ni^{2+} ions. The Lattice constant are calculated according to the subsequent equation:

$$\frac{1}{d^2} = \frac{h^2 + k^2 + l^2}{a^2}$$

Where *d* is the interplanar spacing, (*hkl*) is the miler indices, and *a* is the lattice constant. The lattice constant decreases from 8.362 to 8.345 Å with increasing Ni concentration as shown in Table 1. The crystallite size is likewise calculated from XRD spectra employing the Debye-Scherrer's Formula. Thus, the sample crystallite sizes were determined using the dominant peak (311) to have an average sizes in the range of 20 – 11 nm. The obtained values of lattice constant and particle size for the synthesized ferrites are listed in table 1. As can be seen from the table both particle size and the lattice decrease with an increase in Ni^{2+}. It is observed that the unit cell parameters of the Ni substituted Cu ferrite decrease linearly with increasing concentration of Ni^{2+} ions in the composition, in accordance with the law of Vegard [42]. Fig. 2 displays the variation of the mean crystallite size and lattice parameter with nickel content. The average crystallite size is reduced by increasing the Ni ions in the copper nanoferrites. This lower in Lattice parameter is due to the smaller ionic radii of the Ni^{2+} ion (0.69 Å) as compared to the Cu^{2+} ion (0.73 Å) [43]. This result is trust the ones stated previously [44].

3.2 FT-IR analysis

Two sub-lattices consist of the ideal spinel structure, namely tetrahedral sites (A) and octahedral sites (A) (B). In A and B positions, different charge combinations of metal cations are spread. The magnetic properties of spinel ferrite are, therefore, largely determined by the class of metal ions and the distribution of cations between the A and B sites. In $Cu_{1-x}Ni_xFe_2O_4$ nanofibers, the magnetic properties of samples will be influenced by the substitution of Cu^{2+} ions with Ni^{2+} ions at B sites. FT-IR spectra are typically assigned to crystal lattice ion vibration, which can be used to validate the spinel structure positions of Ni^{2+}, Cu^{2+}, and Fe^{3+} ions.

Fig. 3 displays the FTIR spectra of $Cu_{1-x}Ni_xFe_2O_4$ (x= 0.0, 0.2, 0.6 and 1.0) within the range 400-3000 cm^{-1}. The infrared transmittance spectra of the prepared samples have been investigated to draw information about the structure and types of bonds present in the sample. In mixed ferrites, two essential broad metal-oxygen bands are found in the FTIR spectra and are called as tetrahedral (A-site) and octahedral (B-site). The highest band ν_1 refers to the intrinsic stretching vibrations of the metal and oxygen atoms at the tetrahedral site (Mtetra- O) and is usually observed in the range of 542 to 555 cm^{-1}. While the lowest band ν_2 corresponds to the stretching vibrations of the metal at the octahedral site (Mocta - O) [45] and is normally located in the range 454 - 470 cm^{-1}. It is observed that ν_1 and ν_2 band shifts towards the higher frequencies with in Ni^{2+} ion concentration. Then the octahedral sites are

fully occupied by nickel ions and with increasing content of Ni^{2+} ions, the Fe^{3+} are forced at tetrahedral sites to replace copper ions.

Our FTIR spectra is in a good agreement with those obtained in previous literatures [23,50]. The difference in the location of the ν_1 and ν_2 bands can be related to the difference in Fe^{3+}- O^2 bond lengths at A sites and B sites. It was found that the Fe-O distance at the A sites (1.89 Å) was found to be lower than that at the B sites (2.03 Å) [24,46]. As Cu^{2+} ions are replaced by Ni^{2+} ions, some Fe3+ ions move from A sites to B sites due to charge imbalance, increasing the Fe^{3+}- O^2 stretching vibration.

3.3 Transmission electron microscopy (TEM) studies

Fig. 4 and Fig. 5 shows the morphology and histrograms of the $Cu_{1-x}Ni_xFe_2O_4$ system (x= 0.2, 0.4, 0.6, 0.8 and 1.0). TEM images of Cu-Ni samples (Fig. 4(a – f)) show that all samples in agglomeration display as spherical shaped particles. Fig. 5A shows that $CuFe_2O_4$ nanoparticles are pure, and Fig. 4(b – f) shows the images of the homogeneous and agglomerated Cu-Ni.nanoferrires. Due to the magnetic interactions among the particles, nanoparticles are agglomerated [47]. Fig. 5(a-f) display the histograms of the samples and their average particle size ranging from 24 to 11.5 nm for Ni-doped $CuFe_2O_4$ samples. Fig. 5 shows that the size of nanoparticles of $Cu_{1-x}Ni_xFe_2O_4$ decreases when the concentration of nickel is increased. The sizes correspond well with crystallite sizes obtained from XRD data.

3.4 Energy dispersive X-ray spectroscopy (EDX) analysis

EDX analysis is employed for the chemical analysis of (x= 0.2, 0.4, 0.6, 0.8 and 1.0) nanoparticles and is viewed in Fig. 6(a-e). Fig. 6a shows the peaks of the elements Fe, Cu and O in pure $CuFe_2O_4$. Fig. 6(b–e), displays the peaks of Fe, Cu, Ni and O elements for Ni-doped $CuFe_2O_4$ samples. EDX results match perfectly with XRD data. The experimental conditions completely favor the formation of mixed ferrite. The findings support the formation of $CuFe_2O_4$ and Ni-doped $CuFe_2O_4$ impurities.

3.5 UV-Vis absorption studies

The UV-Vis optical spectrums of $Cu_{1-x}Ni_xFe_2O_4$ nanoferrites recorded in the wavelength range 240 nm -700 nm are shown in Fig. 7. The absorption band is moved to shorter wavelength when Ni is substituted in copper ferrites, suggesting an increase in band gap energy as shown in Fig. 7. In order to determine the value of the optical band gap of the synthesized $Cu_{1-x}Ni_xFe_2O_4$ ferrite nanoparticles, fundamental absorption, which corresponds to electron excitation from the valance band to conduction band, may be used. The optical band gap energy (E_g) for prepared samples was calculated from the extrapolation of linear part of Tauc's relation is given [48] as:

$$(\alpha h\nu) = \sqrt{A(h\nu - E_g)} \qquad (2)$$

where α, h, ν, E_g, and A are the absorption coefficient, Plank's constant, light frequency, band gap, and proportionality constant, respectively. For the estimation of E_g for direct electronic transition in $Cu_{1-x}Ni_xFe_2O_4$ nanoferrites, $(\alpha h\nu)^2$ is plotted as a function of energy ($h\nu$) in Fig. 8. The determined values of $Cu_{1-x}Ni_xFe_2O_4$ band gap ranged from 3.32 to 3.62 eV. Copper ferrite has a band gap value of 3.32 eV, and nickel ferrite is 3.62 eV. This can be demonstrated using the effective mass model of the Bras [49], which allows the measured band gap to express an inverse function of particle size. The band gap energy in these samples increases with increased concentration of Ni^{2+}. Raji et al. [50], Wang et al. [51], Chen et al. [52] and Hossain et al. [53] observed the same effect. Multiple parameters such as impurities, carrier concentrations, crystallite thickness, and lattice strain can lead to an increase in the optical band gap by injecting Ni^{2+} ions into $CuFe_2O_4$ ferrites. In this case, variations in the optical band gap are caused by the sp-d interaction between the $CuFe_2O_4$ and the band electrons and the located d electrons of divalent nickel ions [54–58].

3.6 Magnetic Measurements

The replacement of Cu^{2+} by Ni^{2+} was chosen because magnetic nickel ions inside the spinel structure tend to occupy the octahedral B site [59]. The mentioned nickel-copper ferrite studies have proven that Ni^{2+} ions are placed only in the octahedral region, while Cu^{2+} ions that occupy both A and B sites. It is well-known that magnetic

interactions and distribution of cations in the tetrahedral and octahedral sites affect the structural and magnetic properties of spinel ferrites [60]. In the present study, the hysteresis loops of $Cu_{1-x}Ni_xFe_2O_4$ (x= 0.0, 0.2, 0.4, 0.6, 0.8, and 1.0) are measured using SQUID at room temperature. The magnetic hysteresis loops of the nanoferrites are displayed in Fig. 9. The hysteresis loops show the features of soft magnetic materials. The various parameters such as saturation magnetization (M_s), remanent (M_r), coercivity (H_c), (M_r / M_s) and magnetic moment (μ_B) were tabulated in Table 2. It referred to that the rise in Ni^{2+} concentration results in a rise in M_s and a decrease in H_c, which is due to the ferrite cation distribution (see Fig. 10). It is noted that with an increase in nickel substitution, Ms and Mr are increasing. As seen in Table 2, the M_s increases from 20.35 to 54.3 $emug^{-1}$ as x rises from 0 to 1.0 (see Figure 10). The rise in saturation magnetization has been due to Ni^{2+} ions having a greater magnetic content (2.3 μB) than Cu^{2+} ions (1 μB) [61]. Therefore, the magnetic moment in the B-sub lattice was sequentially increased with an increase in nickel doping resulting in an overall increasing in the magnetic moment of the Ni^{2+} ion doping samples. The increase in M_s with Ni^{2+} content can be clarified by the possible replacement of Cu^{2+} by Ni^{2+} at the tetrahedral sites. These found trends in the variant of M_s can be justified by means of Neel's two sub-lattice magnetization model [62,63]. This model is based on, magnetization (in μ_B) is given by means of $M(\mu_B) = M_B - M_A$, where M_A and M_B are the net magnetic moments of A (tetrahedral) and B (octahedral) sites, respectively. The introduction of Ni^{2+} ions at A-site causes Fe^{3+} ions to move from A to B site, thereby increasing the concentration of Fe^{3+} ions at B-sites, which in turn increases the magnetic moment of B site. This results in an increase in the number of spins on B site, resulting in an increase in net magnetization [64]. However, the super-exchange interaction between A and B sites increases with increasing Ni^{2+} content. The heavy interaction of exchange between sites A and B can be due to an increase in saturation magnetization [63]. Therefore, the increase trend in saturation magnetization and magnetic moment is agreed with that of a predicted increase in $Cu_{1-x}Ni_xFe_2O_4$ nanoferrites [33]. In order to calculate the magnetic moment (μ_B) in Bohr, the following relationship is calculated [65] and represented in Table 2.

$$\eta_B = \frac{M \times M_s}{5585} \qquad (4)$$

Where 'M' denotes molecular weight and 'Ms' denotes saturation magnetization. The rise in values arising from the strong super-exchange interactions between the various sites contributed to an increase in the values. In our case, η_B was observed to increase with increasing Ni^2 content, as well as the saturation magnetization (see Fig. 11). Moreover, with an increase in Ni content, the ratio between Mr and Ms (Mr / Ms) decreased too. Table 2 displays the values of
Mr / Ms for ferrites $Cu_{1-x}Ni_xFe_2O_4$ ranging from 0.36 to 0.024. Such values are less than the predicted standard value of "1.0" for ferromagnetic samples of single domain. The observed deviation from unity (1) could be due to interactions between the grains caused by the distribution of grain size in the material [66-68].

4 CONCLUSIONS

$Cu_{1-x}Ni_xFe_2O_4$ nanoferrites were prepared by using a co-precipitation method to investigate the role of nickel substitution in sterilization the physical properties of copper ferrites. Variability of nickel substitution has a valuable effect on the optical properties, grain size, and magnetics. X-ray diffraction and the Fourier transform infrared (FTIR) analysis confirmed a single-phase cubic spinel structure. However, lattice constant decreases with increasing in nickel concentration due to the substitution of Ni^{2+} of smaller cation radius, though particle size varies in significantly. When the concentration of Ni increased, the size of the nanoparticles decreased from around 20 to around 11 nm. The band gap energy of nanoferrites increases from 3.32 to 3.62 eV with the increase of Ni^{2+} ion. Saturation magnetization and remanent magnetization are gradually increases when Ni^{2+} substitutes Cu^{2+}. The results obtained for the modification and the tunable magnetic properties of synthesized nanoparticles can be suggested for future applications.

Figure Captions:

Fig. 1. XRD analysis of $Cu_{1-x}Ni_xFe_2O_4$ nanoferrites.
Fig. 2. Variation of average particle size and Lattice parameter as a function of Ni content.
Fig. 3. FT-IR spectra of $Cu_{1-x}Ni_xFe_2O_4$ (a) x = 0.0, (b) x = 0.2, (c) x=0.6 and (d) x=1.0

Fig. 4. TEM micrographs of $Cu_{1-x}Ni_xFe_2O_4$ (a) x= 0.0, (b) x= 0.2, (c) x= 0.6 and (d) x= 0.8 and (e) x= 1.0.
Fig.5. Histograms of $Cu_{1-x}Ni_xFe_2O_4$ (a) x= 0.0, (b) x= 0.2, (c) x= 0.6 and (d) x= 0.8 and (e) x= 1.0.
Fig. 6. EDX spectrum of $Cu_{1-x}Ni_xFe_2O_4$ (a) x = 0.0, (b) x = 0.2, (c) x = 0.4, (d) x= 0.6 and (e) x = 0.8.
Fig. 7. UV-vis. spectra of $Cu_{1-x}Ni_xFe_2O_4$ (x= 0.0, 0.2, 0.4, 0.6, 0.8 and 1) system.
Fig. 8. Energy gap spectra of $Cu_{1-x}Ni_xFe_2O_4$ nanoferrite.
Fig. 9 Magnetic hysteresis loops of $Cu_{1-x}Ni_xFe_2O_4$ (x = 0.0, 0.2, 0.4, 0.6 and 0.8) system.
Fig. 10. Saturation magnetization Ms and coercivity H_c versus copper content x in $Cu_{1-x}Ni_xFe_2O_4$.
Fig. 11. M_r versus copper content x in $Cu_{1-x}Ni_xFe_2O_4$.

References

[1] Gaba S., Kumar A., Rana P. S., Arora M., Influence of La^{3+} ion doping on physical properties of magnesium nanoferrite for microwave absorption application, J. Magn. Magn. Mater. **460**, 69-77 (2018).
[2] Kefeni K. K., Msagati T. A. M., and Mamba B. B. Ferrite nanoparticles: synthesis, characterization and applications in electronic device. Mater. Sci. Engg. **B 215**, 37-55 (2017).
[3] Talaat M. Hammad, Jamil K. Salem, S. Kuhn, Nadia Abu Shanab, R. Hempelmann. Influence of pluronic P123 in modifying the morphological and optical properties of PbS nanocomposite`` J Mater Sci: Mater Electron 27 (2016) 4186–4193
[4] Sundararajan M, Sailaja V., Kennedy L. J. and Vijaya J. J. Photocatalytic degradation of rhodamine B under visible light using nanostructured zinc doped cobalt ferrite: Kinetics and mechanism. Ceram. Int. **43**, 540-548 (2017).
[5] Akhtar M. N., Rahman A., Sulong A. B. and Khan M. A. Structural, spectral, dielectric and magnetic properties of nanosized ferrite for microwave absorption and high frequency applications. Ceram. Int. **43**, 4357- 4365 (2017).
[6] Pour S. A., Shaaterian H. R., Afradi M. and El-Ebadi A. Y. Carboxymethyl cellulose (CMC) loaded Co-Cu doped manganese ferrite nanorods as a new dual modal simultaneous contrast agent for magnetic resonance imaging and nanocarrier for drug delivery system. J. Magn. Magn. Mater. **438**, 85-94 (2017).
[7] Mohapatra, J., et al., Surface controlled synthesis of MFe_2O_4 (M= Mn, Fe, Co, Ni and Zn) nanoparticles and their magnetic characteristics. Cryst. Eng. Comm, **15**, 524-532 (2013).
[8] Patade, S.R., et al., Preparation and Characterizations of Magnetic Nanofluid of Zinc Ferrite for Hyperthermia Application. Nanomaterials and Energy **9**, 1-7 (2020).
[9] Talaat M. Hammad, Jamil K. Salem, S. Kuhn, Mohammed Abu Draaz, R. Hempelmann, Fawzi S. Kodeh "Optical properties of Cu^{2+} and Fe^{2+} doped ZnS semiconductor nanoparticles synthesized by co-precipitation method" J Mater Sci: Mater Electron 26 (2015) 5495- 5501.
[10] Talaat M. Hammad, S. Kuhn, Ayman Abu Amsha, Nasser K. Hejazy, R. Hempelmann, comprehensive study of the impact of Mg^{2+} doping on optical, structural, and magnetic properties of copper nanoferrites, Journal of Superconductivity and Novel Magnetism. https://doi.org/10.1007/s10948-020-05559-2
[11] Talaat M. Hammad, S. Kuhn, Ayman Abu Amsha, R. Hempelmann, Investigation of structural, optical, and magnetic properties of Co^{2+} ions substituted $CuFe_2O_4$ spinel ferrite nanoparticles prepared via precipitation approach, Journal of the Australian Ceramic Society **57** (2021) 543-553.

[12] Bharati, V., et al., Influence of trivalent Al–Cr co-substitution on the structural, morphological and Mössbauer properties of nickel ferrite nanoparticles. Journal of Alloys and Compounds, **821**, 153501 (2020).

[13] A. Manikandan, J. Judith Vijaya and L. John Kennedy, Phys. E, **49,** 117–123 (2013) .
[14] D. Maruthamani, S. Vadivel, M. Kumaravel, B. Saravanakumar, P. Bappi, S. Sankar Dhar, A. Habibi- Yangjeh, A. Manikandan and G. Ramadoss, J. Colloid Interface Sci., **498**, 449-459 (2017).
[15] S. Asiri, M. Sertkol, S. Guner, H. Gungunes, K. M. Batoo, T. A. Saleh, H. Sozeri, M. A. Almessiere, A. Manikandan and A. Baykal, Ceram. Int., **44**, 5751–5759 (2018).
[16] G. Mathubala, A. Manikandan, S. Arul Antony and P. Ramar, Nanosci. Nanotechnol. Lett., **8,** 375–381 (2016).
[17] W. Bayoumi, J. Mater. Sci., 2007, 42, 8254–8261. 18 N. M. Deraz and A. Alari, J. Anal. Appl. Pyrolysis **94**, 41–47 (2012).
[18] A. Silambarasu, A. Manikandan and K. Balakrishman, J. Supercond. Novel Magn., **30**, 2631–2640 (2017).
[19] A. T. Ravichandran, J. Srinivas, R. Karthick, A. Manikandan and A. Baykal, Ceram. Int., **44**, 13247–13252 (2018).

[20] S. Rajmohan, V. Jeseentharani, A. Manikandan, J. Pragasam, Nanosci. Nanotechnol. Lett., **8**, 393–398 (2016).
[21] W.H. Bragg, Philos. Mag. **30**, 305 (1915).
[22] S.E. Shirsath, B.G. Toksha and K. M. Jadhav, Mater. Chem. Phys. **117**, 163 (2009).
[23] Al-Ghamdi A. A., Al-Hazmi F. S., Memes L. S., Shokr F. S. and Bronstein L. M. Evolution of the structure, magnetic and optical properties of $Ni_{1-x}Cu_xFe_2O_4$ spinel ferrites prepared by soft mechanochemical method. J. Alloys Compd. **712**, 82-89 (2017).
[24] Skandan G., Hahn H., Roddy M. and Carnnon W. R. Ultrafine-Grained Dense Monoclinic and Tetragonal Zirconia. J. Am. Ceram. Soc. **77**, 1706 (1994).
[25] Boobalan T., Pavithradevi S., Suriyanarayanan N., Raja M. M. and Kumar E. R. Preparation and characterization of polyol assisted ultrafine Cu-Ni-Mg-Ca mixed ferrite via co-precipitation method. J. Magn. Magn. Mater. **428**, 382-389 (2017).
[26] Babu K. R., Rao K. R. and Babu B. R. Cu^{2+} - modified physical properties of cobalt-nickel ferrite. J. Magn. Magn. Mater. **434**, 118-125 (2017).
[27] Das P. S. and Singh G. P. Structural, magnetic and dielectric study of Cu substituted NiZn ferrite nanorod. J. Magn. Magn. Mater. **401**, 918-924 (2016).
[28] Gholizadeh A. and Jafari E. Effect of sintering atmosphere and temperature on structural and magnetic properties of Ni-Cu-Zn ferrite nano-particles: Magnetic enhancement by a reducing atmosphere. J. Magn. Magn. Mater. **422**, 328-336 (2017).
[29] B. K. Bammannavar, L. R. Naik and R. B. Pujar, Prog. Electromagnet. Res. Lett., **4**, 121–129 (2008).
[30] H. Mohseni, H. Shokrollahi, I. Sharifi and K. Gheisari, Magnetic and structural studies of the Mn-doped Mg–Zn ferrite nanoparticles synthesized by the glycine nitrate process, J. Magn. Mater. Mater. **324,** 3741-3747 (2012).
[31] R. Lontio, P. Kenfack, D. Magnin, S. Hermans, A. Delcorte and J. Lambi, J. Solid State Chem., **230**, 381–389 (2015).
[32] Nguyen Kim Thanh, To Thanh Loan, Luong Ngoc Anh, Nguyen Phuc Duong, Siriwat Soontaranon, Nirawat Thammajak, Than Duc Hien, Cation distribution in $CuFe_2O_4$ nanoparticles: Effects of Ni doping on magnetic properties, JOURNAL OF APPLIED PHYSICS **120**, 142115 (2016).
[33] Adil Saleem, Yujun Zhang, Hongyu Gong, Muhammad K Majeed, Xiao Lin, M Muzammal Hussain, M Zeeshan Ashfaq, Mater. Res. Express **7**, 016117 (2020).
[34] S.G. Doha, E.B. Kimb, B.H. Leeb, J.H. Oh, J. Magn. Magn. Mater. **272–276**, 2238 (2004).
[35] J. Azadmanjiri, H.K. Salehani, M.R. Barati, F. Farzan, Mater. Lett. **61,** 84 (2007).
[36] Kh. Roumaih, J. Alloys Compd. **465**, 291 (2008).
[37] J. Msomi, T. Moyo, J. Magn. Magn. Mater. **321**, 1246 (2009).
[38] Talaat M. Hammad, Jamil K. Salem, Ayman Abu Amsha, Nasser K. Hejazy, Journal of Alloys and Compounds **741,** 123-130 (2018).
[39] F.S. Tehrani, V. Daadmehr, A.T. Rezakhani, R.H. Akbarnejad, S. Gholipour, J. Supercond. Novel Magn. **25**, 2443–2455 (2012).
[40] C. Luadthong, V. Itthibenchapong, N. Viriya-empikul, K. Faungnawakij, P. Pavasant, W. Tanthapanichakoon, Mater. Chem. Phys. **143**, 203–208 (2013).
[41] S.A. Masti, A.K. Sharma, P.N. Vasambekar, Adv. Appl. Sci. Res. **4**, 163–166 (2013)
[42] Q. A. Pankhurst, J. Connolly, S. K. Jones, and J. J. Dobson, J. Phys. D: Appl. Phys. **36**, R167 (2003).
[43] J. Z. Jiang, P.Wynn, S. Morup, T. Okada, F. J. Berry, Nanostructured Materials **12**, 737 (1999).
[44] Nguyen Kim Thanh, To Thanh Loan, Luong Ngoc Anh, Nguyen Phuc Duong, Siriwat Soontaranon, Nirawat Thammajak, Than Duc Hien, JOURNAL OF APPLIED PHYSICS, **120,** 142115 (2016).
[45] Naidu V. Study of Electrical & Magnetic properties in Nanosized Ce-Gd Doped Magnesium Ferrite. Int. J. Computer Appl. **27**, 0975 (2011).
[46] S.A. Mazen, M.H. Abdallah, B.A. Sabrah, H.A.M. Hashem, Phys. Status Solidi (a) **134**, 26 (1992).
[47] S. Rahman, K. Nadeem, M.A. Rehman, M. Mumtaz, S. Naeem, I.L. Papst, Structural and magnetic properties of ZnMg-ferrite nanoparticles prepared using the co-precipitation method, Ceram. Int. **39**, 5235–5239 (2013).
[48] Talaat M. Hammad, Jamil K. Salem, Nadia Abu Shanab, S. Kuhn, R. Hempelmann, surface morphological and optical properties of PVA passivated PbS nanoparticles, Journal of Luminescence **157**, 88–92 (2015).
[49] J. Judith Vijaya, G. Sekaran, and M. Bououdina, Ceram. Int. 41, 15 (2014).
[50] B. Gayathri Manju and P. Rajh, Green Synthesis of Nickel–Copper Mixed Ferrite Nanoparticles: Structural, Optical, Magnetic, Electrochemical and Antibacterial

Studies, Journal of ELECTRONIC MATERIALS. https://doi.org/10.1007/s11664-019-07603-x
[51] Y.S. Wang, P.J. Thomas, P. Brien, Optical properties of ZnO nanocrystals doped with Cd, Mg, Mn, and Fe ions, J. Phys. Chem. **B 110**, 21412 (2006). https://doi.org/10.1021/jp0654415.
[52] Z.C. Chen, L.J. Zhuge, X.M. Wu, Y.D. Meng, Initial study on the structure and optical properties of $Zn_{1-x}Fe_xO$ films, Thin Solid Films **515**, 5462-5465 (2007).
[52] A.S. Ahmed, S.M. Muhamed, M.L. Singk, S. Tabassum, A.H. Naqvi, A. Azam, Band gap narrowing and fluorescent properties of nickel doped SnO2 nanoparticles, J. Lumin. **131**, 1-6 (2011).
[53] Mohammad Sajjad Hossain, Yeasmin Aktery, Mohammad Shahjahany, Muhammad Shahriar Basharz, Influence of Ni substitution on structural, morphological, dielectric, magnetic and optical properties of Cu–Zn ferrite by double sintering sol–gel technique, JOURNAL OF ADVANCED DIELECTRICS, 9 (2019) 1950020.
[54] A. Manikandan, M. Durka, S.A. Antony, one-pot flash combustion synthesis, structural, morphological and opto-magnetic properties of spinel $Mn_xCo_{1-x}Al_2O_4$(x =0,0.3 and 0.5) nanocatalysts, J. Supercond. Nov. Magn. **28**, 209-218 (2015).
[55] A. Manikandan, M. Durka, S.A. Antony, Role of Mn^{2+} doping on structural, morphological, and opto-magnetic properties of spinel $Mn_xCo_{1-x}Fe_2O_4$(x = 0.0, 0.1, 0.2, 0.3, 0.4, and 0.5) nanocatalysts, J. Supercond. Nov. Magn. **28**, 2047-2058 (2015).
[56] A.A. Godlyn, A. Manikandan, E. Manikandan, S.K. Jaganathan, A. Baykal, P. Sri Renganathan, Enhanced opto-magneto properties of $Ni_xMg_{1-x}Fe_2O_4$ ($0.0 \leq x \leq 1.0$) ferrites nano-catalysts, J. Nanoelectron. Optoelectron. **12,** 1326-1333 (2017).
[57] A. Manikandan, S.A. Antony, R. Sridhar, S. Ramakrishna, M. Bououdina, A simple combustion synthesis and optical studies of magnetic $Zn_{1-x}Ni_xFe_2O_4$ nanostructures for photoelectrochemical applications, J. Nanosci. Nanotechnol. **15**, 4948-4960 (2015).
[58] W. Pan, F. Gu, K. Qi, Q. Liu, J. Wang, Effect of Zn substitution on morphology and magnetic properties of $CuFe_2O_4$ nanofibers, J. Mater. Chem. Phys. **134**, 1097 (2012).
[59] C. N. Chinnasamy, A. Narayanasamy, N. Ponpandian, K. Chattopadhyay,K. Shinoda, B. Jeyadevan, K. Tohji, K. Nakatsuka, T. Furubayashi, and I.Nakatani, Phys. Rev. **B 63**, 184108 (2001).
[60] H. M. Zaki, Physica **B 407**, 2025 (2012).
[61] S. M. Hoque, A. Choudhury, and F. Islam, J. Magn. Magn. Mater. 251 (2002) 292.
[62] L. N. Anh, T. T. Loan, N. P. Duong, S. Soontaranon, T. T. Viet Nga, and T. D. Hien, J. Alloys Compd. **647**, 419 (2015).
[63] Rais, A., Taibi, K., Addou, A., Zanoun, A. and Al-Douri, Y. Ceramics International **40**, 14413-14419 (2014).
[64] Moradmard H, Farjami Shayesteh S, Tohidi P, Abbas Z and Khaleghi M, Structural, magnetic and dielectric properties of magnesium doped nickel ferrite nanoparticles J. Alloys Compd. 650 (2015) 116–22
[65] Gabal, M.A., Al Angari, Y.M. and Kadi, M.W. Polyhedron **30**, 1185-1190 (2011).
[66] N. Lenin, K. Sakthipandi, R. Rajesh Kanna, and G. Rajkumar, Ceram. Int. **44**, 21866 (2018).
[67] G. Baldi, D. Bonacchi, C. Innocenti, G. Lorenzi and C. Sangregorio, Cobalt ferrite nanoparticles: The control of the particle size and surface state and their effects on magnetic properties, J. Magn. Magn. Mater., 311, 10–16 (2007).
[68] Balavijayalakshmi J, Suriyanarayanan Nand Jayaprakash. R. Role of copper on structural, magnetic and dielectric properties of nickel ferrite nano particles. J. Magn. Magn. Mater. **385,** 302–7 (2015)

Table 1. Lattice constant and particle size of $Cu_{1-x}Ni_xFe_2O_4$.

Composition	0.0	0.2	0.4	0.6	0.8	1.0
Lattice constant (Å)	8.362	8.359	8.357	3.352	8.349	8.342
Particle size (nm)	20	18.4	16.7	14.5	13.2	11

Table 2. The values of magnetic parameters, M_s, Mr, H_c, M_r/M_s and η_B of $Cu_{1-x}Ni_xFe_2O_4$ nanoparticles at x= 0, 0.2, 0.4, 0.6, 0.8, and 1.0

X	**Saturation magnetization** M_S (emu/g)	**Remanent magnetization** M_r (emu/g)	**Coercivity** H_c (Oe)	M_r/M_s	Magnetic moment ηB (μ_B)
0	20.35	7.26	1330	0.36	0.872
0.2	26.6	8.8	1136	0.48	1.14
0.4	34.8	12.5	730	0.45	1.5
0.6	40.2	13.3	700	0.25	1.72
0.8	45.7	14.8	576	0.18	1.96
1.0	54.3	17.05	456	0.024	2.11

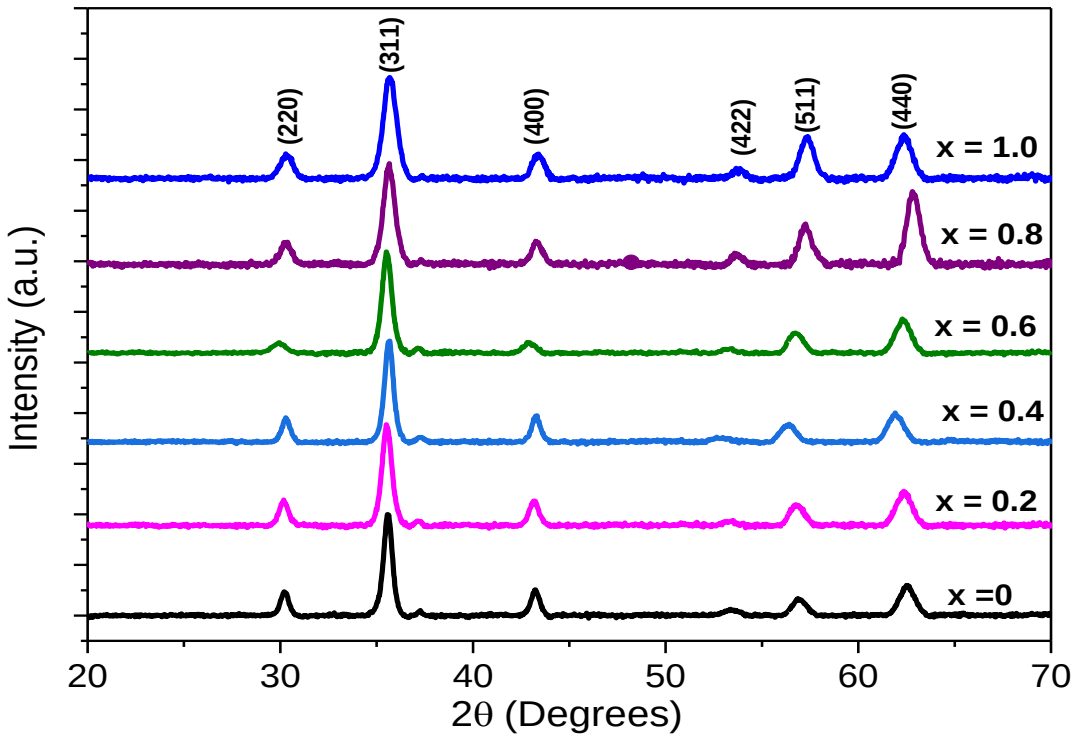

Fig. 1

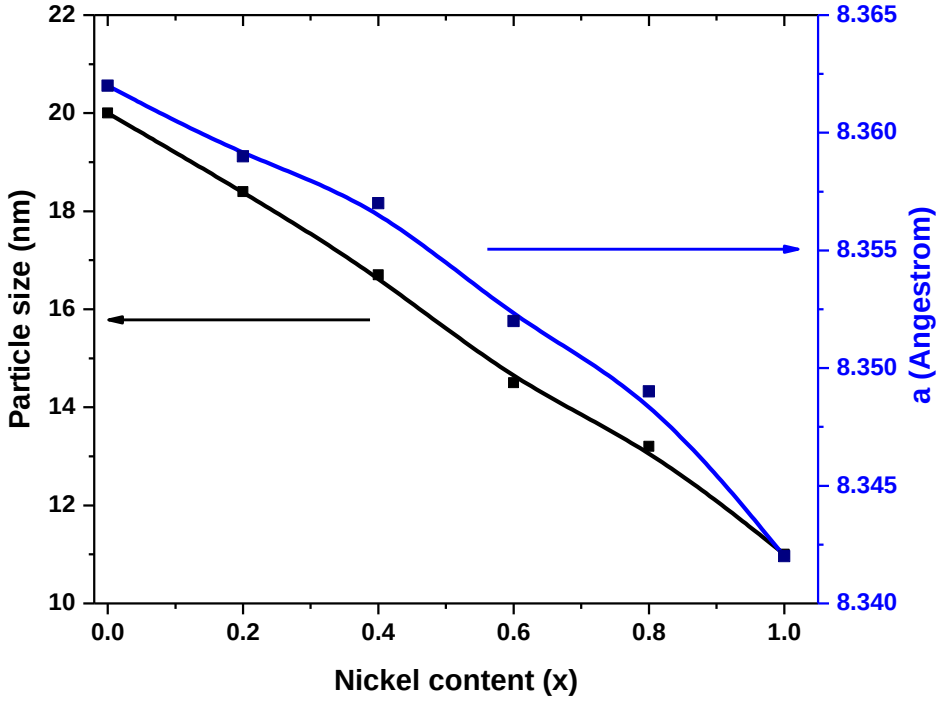

Fig. 2

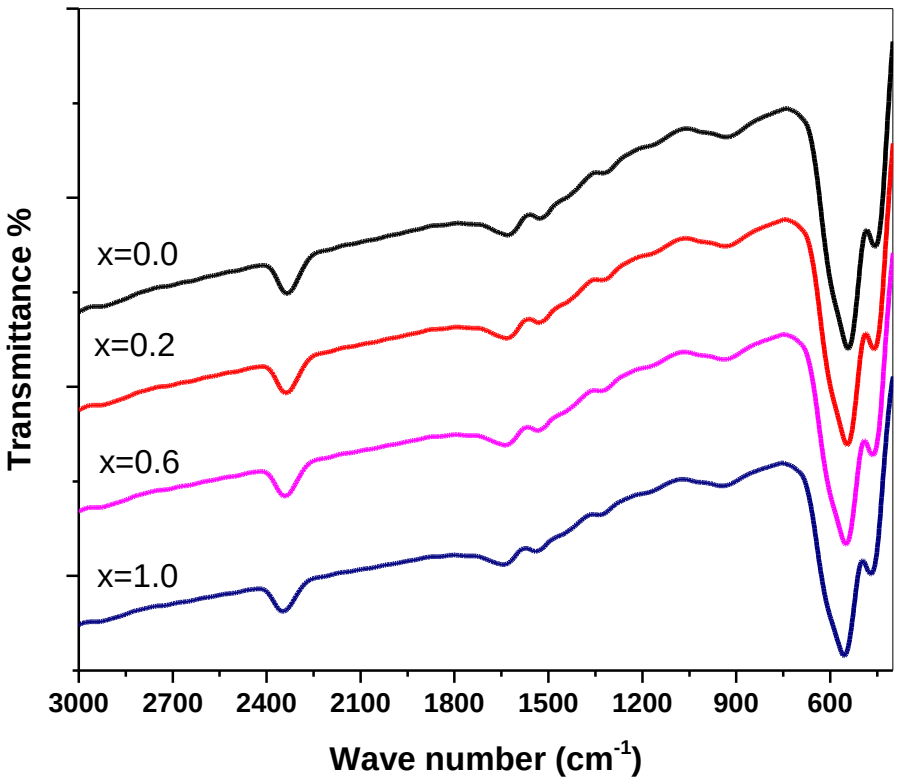

Fig. 3

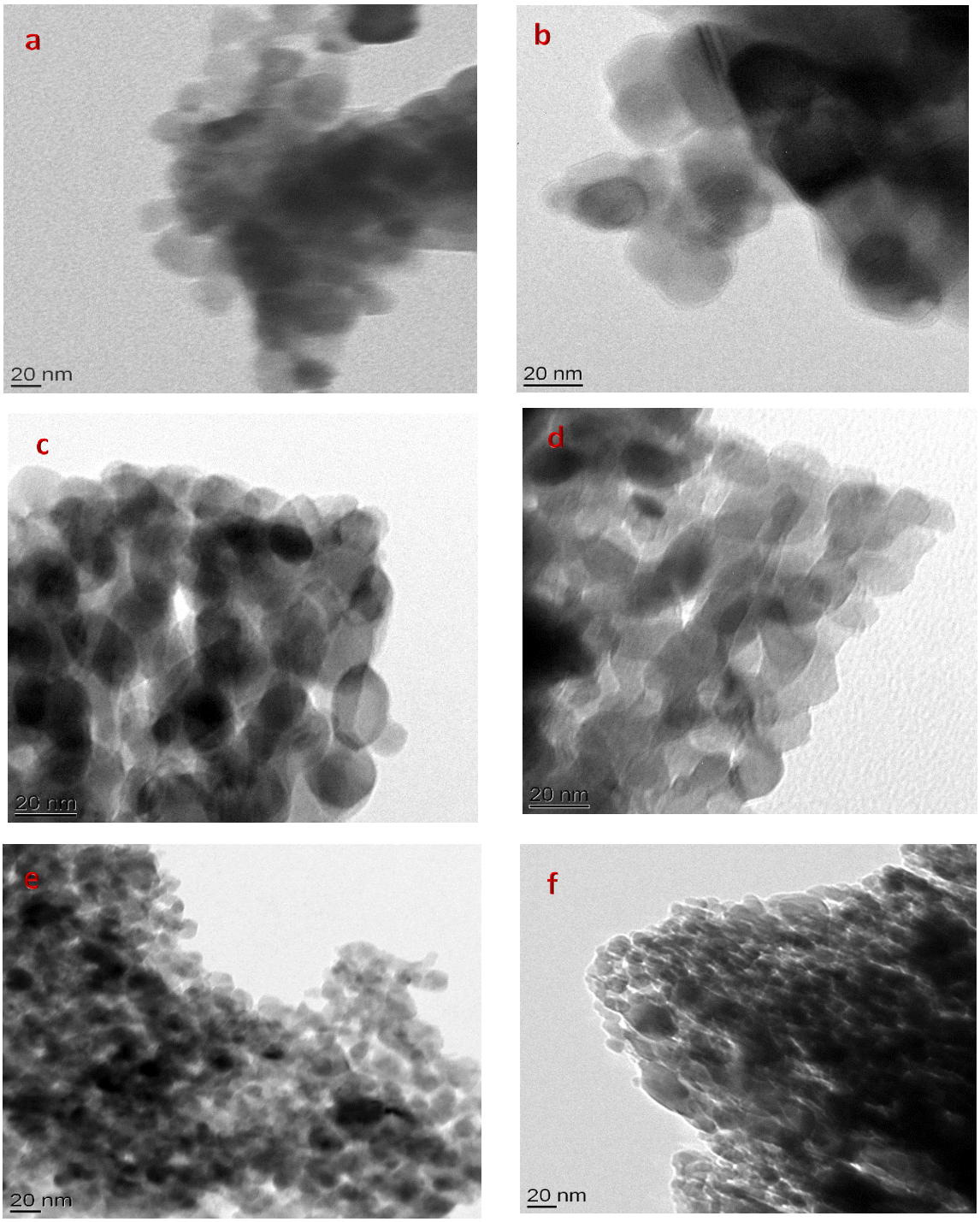

Fig.4 (a-f)

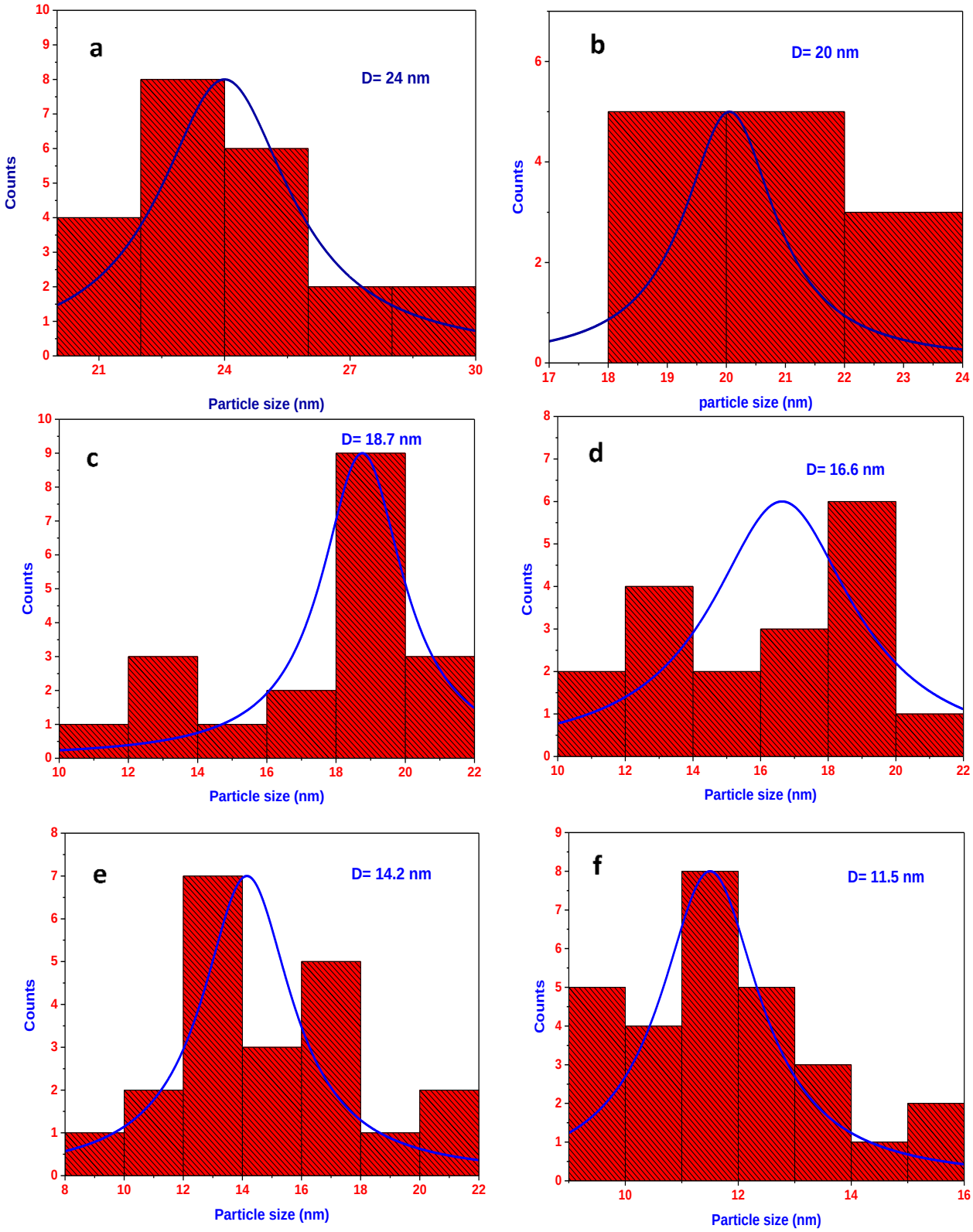

Fig. 5 (a-f)

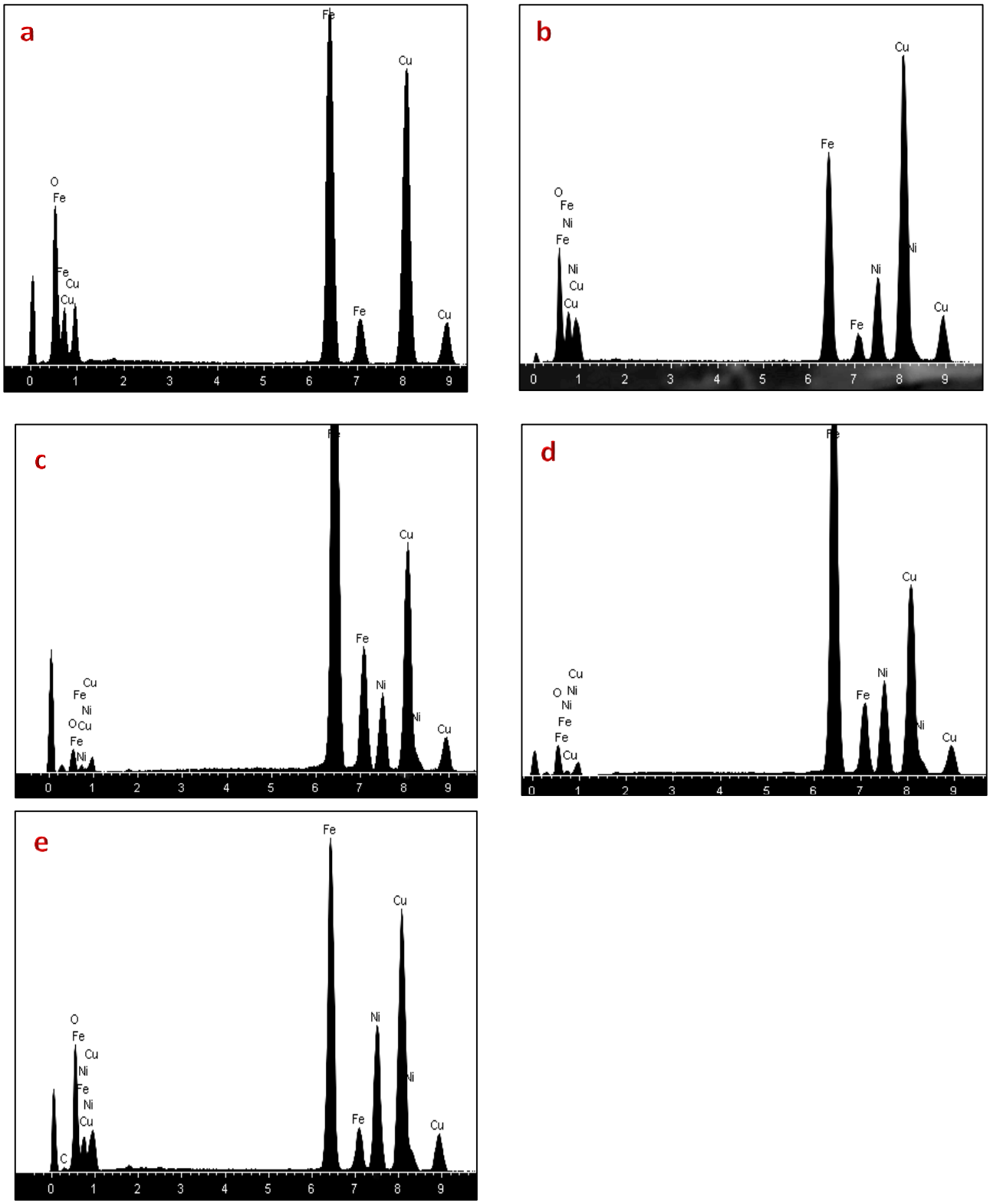

Fig. 6 (a-e)

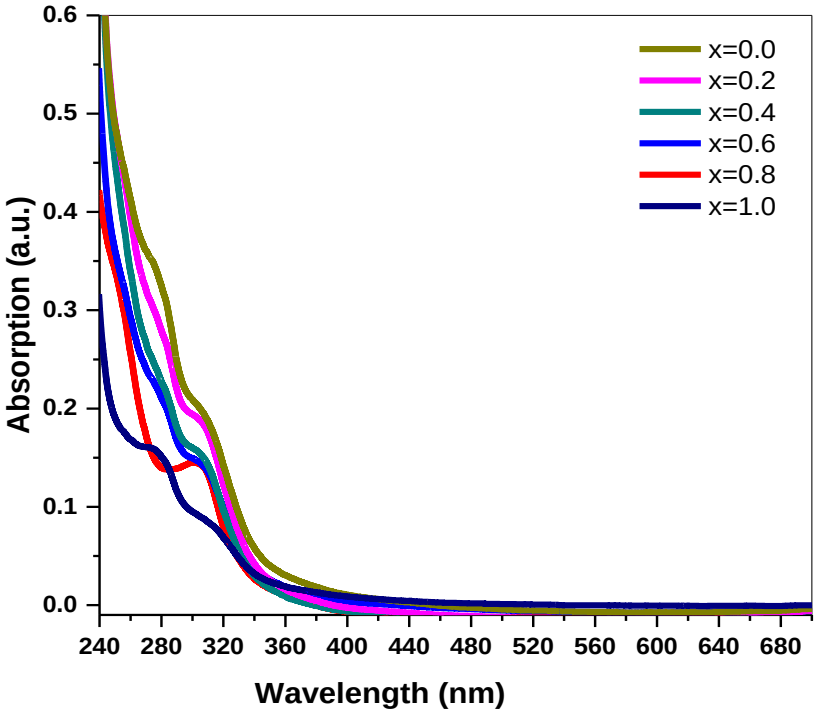

Fig. 7

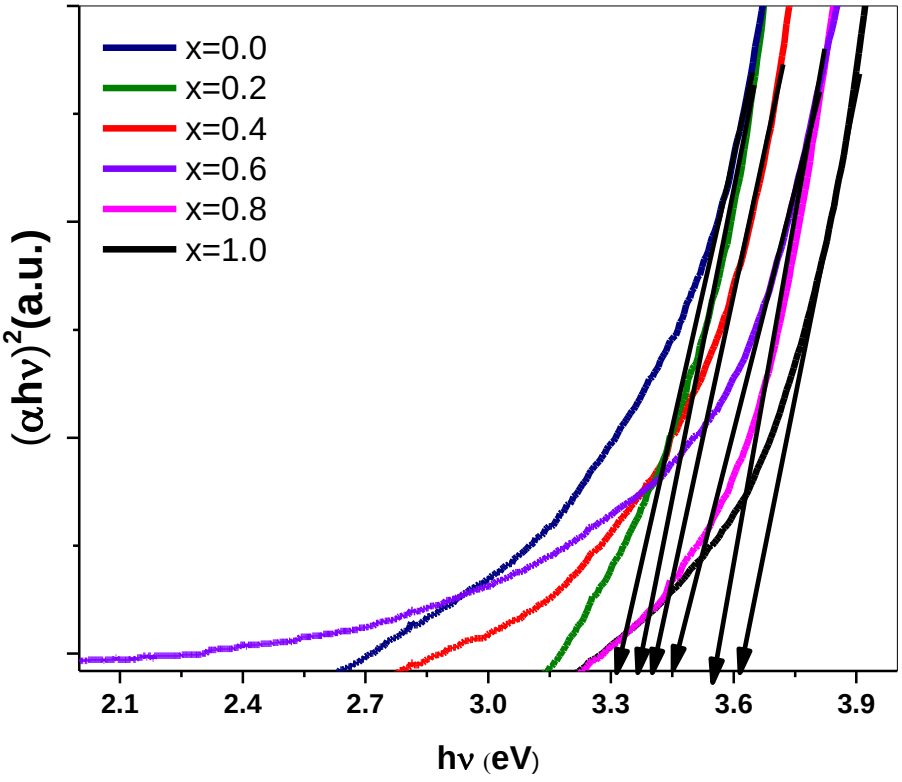

Fig. 8

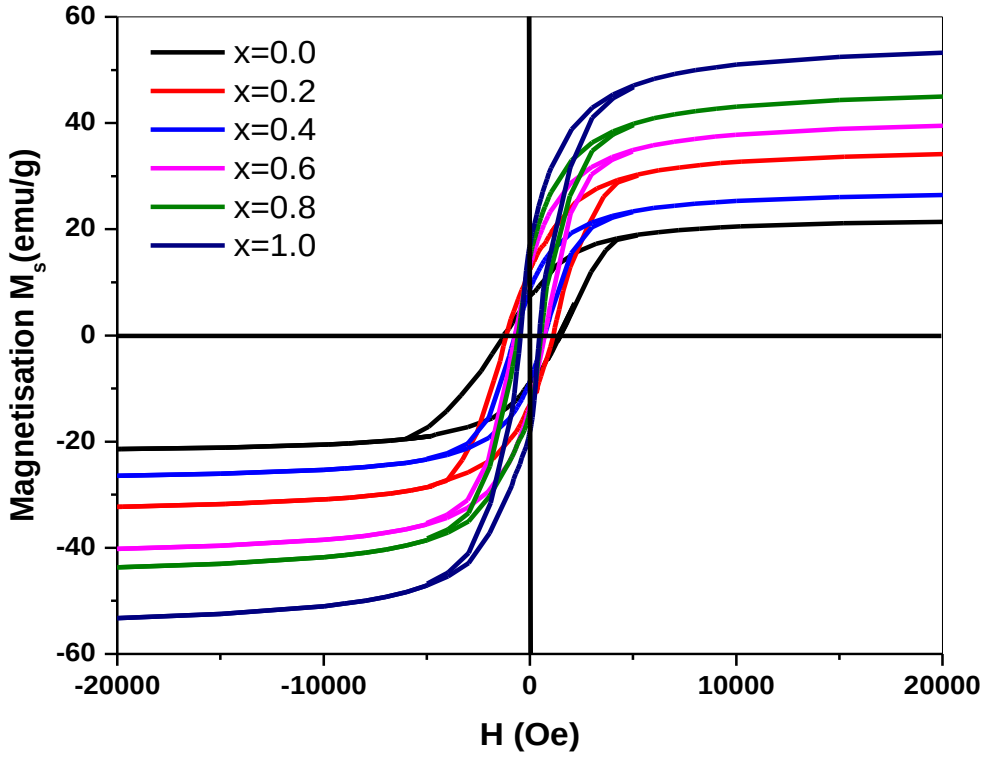

Fig. 9

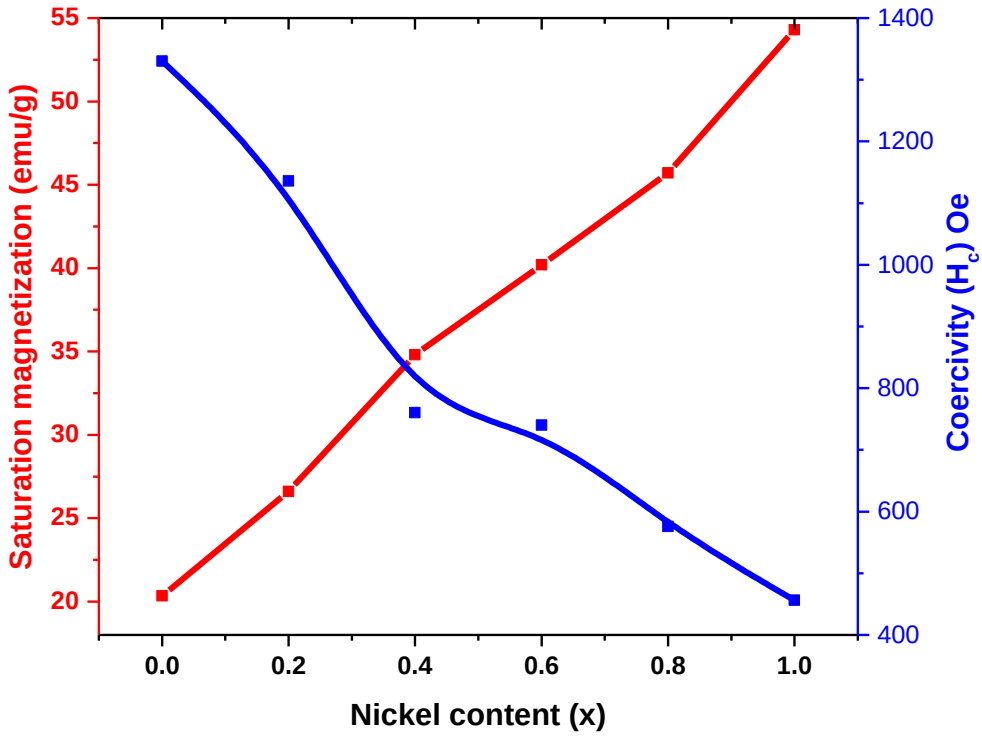

Fig. 10

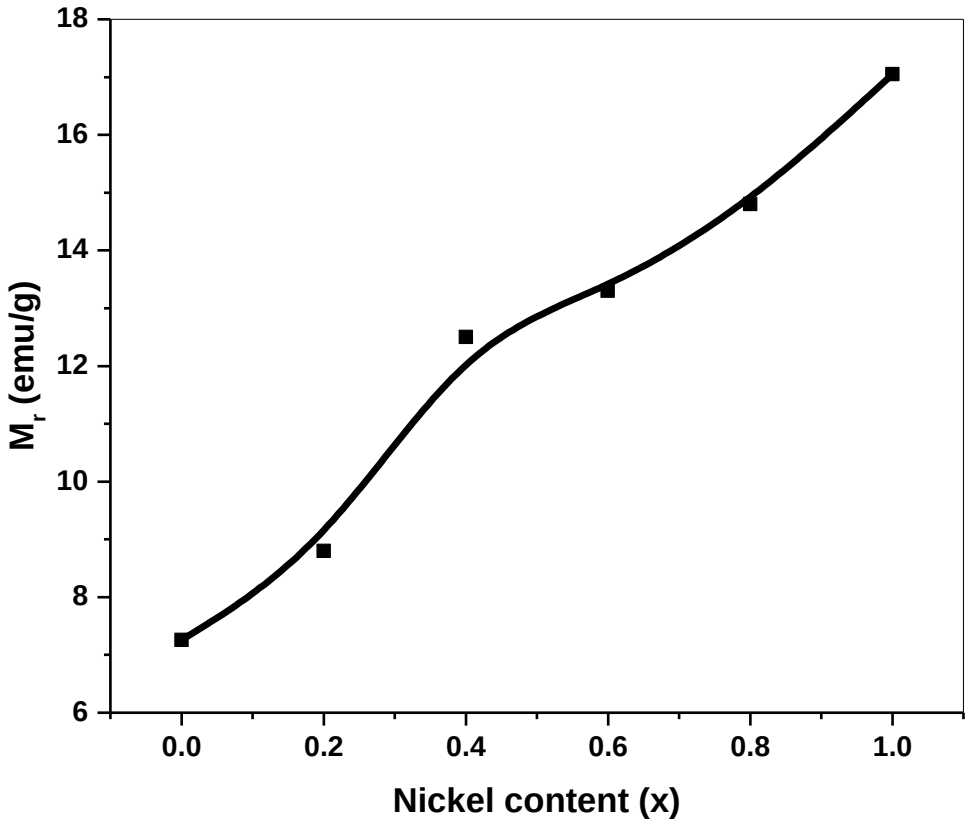

Fig. 11